

**GENETIC CONTROL OF TISSUE SPECIFIC GROWTH IN THE
DROSOPHILA TRACHEA**

By

Erin M. Suderman

Submitted to the graduate degree program in Molecular Biosciences and the
Graduate Faculty of the University of Kansas in partial fulfillment requirements
for the degree of Master of Arts.

Chairperson Robert E. Ward IV

Stuart Macdonald

Kristi L. Neufeld

Date Defended: July 7, 2016

The Thesis Committee for Erin M. Suderman
certifies that this is the approved version of the following thesis:

GENETIC CONTROL OF TISSUE SPECIFIC GROWTH IN THE
DROSOPHILA TRACHEA

Chairperson: Robert E. Ward IV

Date approved: July 7, 2016

ABSTRACT

In most organisms, different tissues and organs grow at different rates relative to each other, suggesting underlying growth mechanisms that act tissue specifically. The mechanisms of tissue specific growth are less well understood than those governing the growth of an entire organism. To gain a better understanding of these tissue specific growth mechanisms, our lab has characterized mutations that specifically alter the growth of the larval trachea in *Drosophila melanogaster*. Larval trachea growth is well suited for these studies since the trachea shows allometric growth during the larval stages, can be imaged and measured in living animals and gene expression can be specifically altered in the trachea using *breathless-GAL4*. Importantly, we and others have identified mutations in genes whose mutant phenotypes suggest that they normally regulate tissue-specific growth in the larval trachea. For example, animals with mutations in *uninflatable (uif)* and *Matrix metalloproteinase 1 (Mmp1)* have larval tracheae that are roughly half the relative size of those in wild type animals. Here we report the results of a screen of EMS-induced larval lethal mutations that recovered seven different alleles that cause either overgrowth or undergrowth of the larval trachea. Three of these mutations form one complementation group, and we have used complementation mapping and RNA interference to show that the affected gene is *CG11340*. This gene encodes a glycine gated chloride channel previously thought to function only in neurotransmitters. We have named this gene *rio* based upon its long and convoluted tracheal phenotype. Here we show its function as a negative growth regulator in the trachea and demonstrate its interaction with the previously characterized positive growth regulators in tracheal specific growth.

ACKNOWLEDGMENTS

Research reported in this thesis was made possible in part by the services of the KU Genome Sequencing Core Laboratory. This lab is supported by the National Institute of General Medical Sciences (NIGMS) of the National Institutes of Health under award number P20GM103638. This project was supported by an Institutional Development Award (IDeA) from the National Institute of General Medical Sciences of the National Institutes of Health under grant number P20GM103418.

I would like to thank Kayla Wilson, Paulo Leal, Alex Matlock, Colin Clay and Kisti Brunsell for their collaboration on some of the work presented here. I would also like to thank Robert Ward, Stuart Macdonald and Kristi Neufeld for serving on my thesis committee. I would especially like to thank Robert Ward for his guidance throughout my thesis work and graduate career and giving me the opportunities to explore a love of science outreach and education. The past and present members of the Ward lab have been a pleasure to work with, both for their scientific input and friendship. Thank you to Reena Rao for being a wonderful scientific role model and pushing me to continue my education. Finally, thanks to my wonderful husband Ryan for both consoling me during setbacks and celebrating successes all while helping to balance our graduate careers with our wonderful son, Luke. Without his support, this work would not have been possible.

TABLE OF CONTENTS

INTRODUCTION	1
MATERIALS AND METHODS	5
RESULTS	8
DISCUSSION	15
REFERENCES	19
TABLES AND FIGURES	23

INTRODUCTION

Organismal growth involves both the regulation of final body size and the proper proportioning of organs and tissues. This requires the precise integration of multiple regulatory mechanisms including patterning, cell proliferation, growth, cell movements, cell death and differentiation (Britton 2000). Post-embryonic development in most species follows allometric growth in which tissues grow at rates relative to each other as opposed to isometric growth where the proportions of the body in the adult are not significantly different from those in the juvenile. Differential growth of body parts including tissues and organs suggests that there must be genetic tissue-specific mechanisms underlying the control of growth in these tissues. Surprisingly, observations of genetic variation in allometric growth are scarce in the literature (P'elebon et al. 2014), and so we have focused our studies on isolating mutants that effect allometric growth in a simple model organism.

Drosophila tracheal system

We have chosen the larval trachea of the fruit fly, *Drosophila melanogaster*, as our model organism to study the growth of tubular structures in multicellular organisms. Both the genetic mechanisms that underlie development, the growth factors and transcription factors controlling branching and the physical structure of the *Drosophila* trachea are conserved in mammalian tubular organs, such as the kidney and lung (Metzger and Krasnow, 1999, Liu et al., 2002). Therefore, discoveries made in the fruit fly are likely to be applicable in vertebrate physiology.

The trachea acts as the respiratory organ for *Drosophila*. It is composed of a tubular epithelial network one cell in thickness. The trachea opens to the outside of the animal at the

spiracles on both the anterior and posterior ends. The two major dorsal trunks run through the body, branching repeatedly to give rise to finer branches that reach into the body tissues (Figure 1). The main function of the trachea is to facilitate the transport of gases to and from the body tissues. This occurs mainly through passive diffusion since the oxygen in the trachea is several orders of magnitude greater than that in the body fluids. Gases are exchanged in the very fine tracheoles that lie at the ends of the branches near their target tissues (Manning and Krasnow, 1993).

The trachea must maintain strength and structural integrity while also being able to move and grow with the animal. In every instar (distinct stage of larval development), a cuticle forms on the apical extracellular matrix (aECM) of the trachea cells organized into evenly spaced ridges called taenidia. The taenidia appear as rings or spirals that are anchored by an underlying actin cytoskeleton (Matusek et al., 2006), and are able to expand their spacing relative to each other as the trachea grows during each instar (Figure 2). An increase in diameter of the trachea is only possible following the shedding of the cuticle during the larval molts (Beitel and Krasnow, 2000). Since the tracheal cuticle is continuous with the rest of the animal's exoskeleton, it is degraded and expelled through the spiracles as the animal molts (Manning and Krasnow, 1993).

The *Drosophila* tracheal system is an ideal model to study tissue specific growth. In many systems, growth and development occur simultaneously, making it difficult to distinguish the effects apart. This is not the case in the *Drosophila* trachea, where growth and development are isolated from each other, facilitating our investigation of growth-specific phenomena. The development of trachea occurs during embryogenesis, such that upon hatching as a first instar larva, the tracheal system of the animal is completely developed and functional. There are no further developmental events in the trachea during larval stages, rather the trachea grows. Cells of the trachea enter an endoreplication cycle where they grow without dividing, which is in

contrast to the imaginal tissues (that will make up the future adult tissues) that grow and divide by mitosis (Makino, 1938). The four days of larval life provide a unique opportunity to specifically study the growth of the organ, as the larva elongates 8-fold before pupariating to undergo metamorphosis.

Effectors of tracheal specific growth

Little is known about the underlying mechanisms that control tissue-specific growth in the larval trachea. Prior to this study, two genes, *uninflatable (uif)* and *Matrix metalloproteinase I (Mmp1)*, were identified that have defects in larval tracheal-specific growth (Zhang and Ward, 2009, Glasheen et al. 2010). *uif* was characterized for its role in tracheal development and growth in *Drosophila*. *uif* encodes a transmembrane protein with a large extracellular domain with eighteen EGF-like repeats and a carbohydrate-binding motif (Zhang and Ward, 2009). *uif* has also been shown to be involved in the canonical Notch signaling pathway, influencing the accessibility of the Notch extracellular domain available for interacting with its ligands on neighboring cells during Notch activation (Xie et al., 2012). Many *uif* mutants show defects in embryonic tracheal inflation, where growth arrests at approximately 50% the normal length of trachea. Although the trachea is smaller than average, it maintains normal patterning.

The *uif* mutant's most notable phenotype is the larval-specific growth defect of their trachea. Larval *uif* mutants have both shortened trachea and defects in their ability to properly molt their tracheal cuticle. The taenidia in these animals are also disorganized likely due to defects between the aECM and apical cellular membrane. The Uif protein is expressed on the apical plasma membrane of the epidermis, foregut, hindgut and salivary gland, but is strongest in the trachea. Studies using RNAi knockdown of *uif* both ubiquitously and tracheal specifically, show that the *uif* has tissue specific effects in the trachea. Knockdown of *uif* in the posterior

compartment of the epidermis did not show a tracheal effect while *uif* knockdown in the trachea recapitulated the mutant phenotype (Zhang et al., 2009).

Mmp1 is required for normal tracheal growth as it is involved in taenidial expansion, tube elongation and the degradation of the cuticle into pieces before being shed during the molts (Page-McCaw et al., 2003). *Drosophila* mutants in *Mmp1* have stretched and broken trachea caused by the inability of the taenidea to expand as the larva grows (Glasheen et al., 2010). *Mmp1* is conserved in vertebrates as extracellular proteases that are unregulated in both cancer and inflammation (Sternlicht and Werb, 2001). The vertebrate *MMP* family is capable of cleaving multiple components of the extracellular matrix and signaling molecules (Egeblad and Werb, 2002).

To better understand the mechanisms by which the larval trachea grows independently of the rest of the body, we use forward genetics to isolate additional effectors of tissue specific growth. We describe a screen of EMS (ethyl methanesulfonate) mutants for tracheal specific growth effectors in the *Drosophila* larva, where both positive and negative regulators of growth were isolated. A total of seven lines were isolated, most notably three alleles of the *CG11340* gene that cause large, convoluted trachea. We have named this gene *rio* and describe its initial characterization.

MATERIALS AND METHODS

Drosophila strains

We maintained our stocks on a cornmeal, yeast, sugar and agar media in a room that fluctuated between 21°C and 22.5°C. We obtained *UAS-CG11340* RNAi (*y¹ v¹; P{TRiP.JF02028}attP2*), *y¹ w^{*}; Mi{MIC}CG11340^{MI11939}/TM3, Sb¹ Ser¹, breathless (btl)-Gal4, daughterless (da)-Gal4, engrailed (en)-Gal4, w¹¹¹⁸* and the third chromosome deficiency kit from the Bloomington *Drosophila* Stock Center. New tracheal overgrowth alleles are EMS-induced larval lethal mutations on the third chromosome reported in Wang et al., (2008). We balanced the tracheal mutant alleles with *TM6, Dfd>YFP*.

Tracheal growth defect screening

Wang et al., (2008) performed the EMS mutagenesis. We performed a screen on the collection of 252 larval lethals identified from their EMS screen by observing non-tubby 2nd or 3rd instar larvae for altered tracheal lengths compared to their heterozygous (mutation/*TM6, Dfd>YFP*) siblings. We then rebalanced these mutations with *TM6, Dfd>YFP* in order to identify mutant larvae by the absence of YFP. We collected newly hatched mutant larva and grew them on separate apple juice plates at 25°C until either second or third instar as judged by their spiracles. To visualize the degree of tracheal defect under a dissection microscope, we mounted individual larvae in halocarbon oil on microscope slides.

Whole genome sequencing

We collected genomic DNA from non-YFP expressing first and second instar larva through homogenization in buffer composed of 20mM EDTA, 100mM NaCl, 1% Triton X-100, 500 mM guanidine-HCl, 10 mM Tris at pH 7.9. We added RNase A (20 mg/mL) and incubated the

lysates for 30 min at 37°C and spun them at 14,000 rpm. We followed a standard DNA purification protocol and measured DNA quantity using the dsDNA Qubit kit (ThermoFisher). We generated standard DNA sequencing libraries and sequenced on an Illumina HiSeq 2500 instrument (Genome Sequencing Facility, University of Kansas). Read depth of all seven genomes ranged from 20-33 and depth of the third chromosome ranged from 46-78. Analysis was performed in CloudMap by the KU sequencing facility.

Lethal phase and phenotypic analysis

We considered larvae that had not pupariated seven days post-hatching as larval lethal mutants. We quantified trachea length defects by collecting non-YFP embryos and growing them on separate apple juice plates at 25°C. We removed larvae at 24h periods over 7 days and mounted in halocarbon oil on microscope slides.

Measurement of body and tracheal length

We placed the larvae in between a microscope slide and coverslip in Halocarbon Oil 700 (Sigma) and heat-killed the larvae by placing the slide on a 95°C heat block for 10 seconds. We used a Nikon eclipse i80 microscope to image the larvae, and body and trachea lengths were measured in ImageJ (Rasband, 1997–2009). Using the multi-line tool, we measured body length as the most anterior to most posterior point. For partial tracheal length, we measured the distance along the dorsal trunk from the posterior spiracles to the transverse connective that was established in body segment four (Figure 3). We determined the ratio of the partial tracheal length to full body length in each larva. We calculated the ratio of partial trachea length to body length every 24h until two days post pupariation of the control animals. We fit the data in both w^{1118} and *rio* mutants to a linear model in order to characterize the tracheal growth rate.

Immunostaining

We dissected the larval trachea by tearing the larvae in half while suspended in PBS. We fixed trachea for staining by incubation in 4% paraformaldehyde in PBS for 20 min. To perform immunostaining we incubated fixed tissues in blocking solution (normal donkey serum in PBS/0.01% TritonX-100, Sigma) overnight at 4°C with the following antibodies: mouse anti-Uif (Zhang 2009) 1:400, mouse anti-Mmp1 (clones 14A3D2 and 3A6B4 from Developmental Studies Hybridoma Bank (DSHB) at the University of Iowa, Iowa City, IA, USA) 1:50, mouse anti-Cor (clones C566.9 and C615.16 from DSHB) 1:400. We obtained secondary antibodies from Jackson ImmunoResearch Laboratories and used them at 1:800 in blocking solution while incubated at room temperature for 4h before washing and mounting in mounting media. We collected images on a Nikon eclipse i80 microscope, adjusting for brightness and contrast and rotated in ImageJ.

Sequence analysis

We performed sequence alignments using HHPred and protein domains and secondary structures predictions were done using SMART and TMHMM.

RESULTS

Genetic screen for new tracheal growth mutants

Past studies of the tracheal specific growth effectors *uif* and *Mmp1* have given us some understanding of the underlying genetic pathways controlling tracheal specific growth, but there is still more to learn. One way to increase our understanding of these pathways is to identify and characterize additional genes that regulate larval tracheal growth. Our lab has attempted to identify more of these genes by using forward genetic screens.

A collection of 252 larval lethal mutations was generated by treatment with 10mM EMS in the Bashirullah lab (Wang et al., 2008). These mutations were confined to the third chromosome and balanced over the dominant marker Tubby (Tb). We initially screened each stock for non-Tb 2nd and 3rd instar larvae with altered tracheal lengths compared to balanced siblings. We rebalanced these stocks with potential defects in tracheal growth over *TM6*, *Dfd>YFP* for further detailed studies, and rescreened them for mutant phenotypes specific to the trachea. We selected seven lines that showed either overgrowth or undergrowth phenotypes in the larvae (Table 1). All of these mutations appear to show normal embryonic tracheal developments (data not shown).

To determine how many genes were represented among these mutants, we crossed the lines together and tested the transheterozygous offspring for genetic complementation. The seven mutants formed five complementation groups, with one group containing three different alleles (*I(3)LL9349*, *I(3)LL16674*, *I(3)LL10756*) (Table 1, Figure 4).

Phenotypic and lethal analysis differs significantly between the five groups. All combinations, with the exception of *I(3)LL15149*, display 100% larval lethality. The degree of penetrance varies by each allele, with the multiallelic complementation group and *I(3)LL15149* having high penetrance (>75% of larvae affected), *I(3)LL5106* and *I(3)LL12265* showing mid

penetrance (25%-75% of larvae affected), and *I(3)LL16636* having low penetrance (<25% of larvae affected). Terminal body size of the homozygous mutants is smaller than their heterozygous siblings in all the lines. Lines *I(3)LL15149* and *I(3)LL16636* have small terminal body sizes that are roughly the size of a healthy second instar larva, whereas lines *I(3)LL5106*, *I(3)LL12265* and the multiallelic complementation group have medium terminal body sizes, roughly two thirds of the normal late third instar larva.

Three of the mutants (*I(3)LL15149*, *I(3)LL16636*, *I(3)LL5106*), each comprising their own complementation group, are characterized as having short, stretched trachea. These lines survive much longer than their heterozygous sibling larva, typically as long as two weeks before dying. Line *I(3)LL15149* differs from the other three short trachea mutants because the trachea appear brittle and are prone to breaking. Uniquely, these larva pupariate after an extended larval life of nearly two weeks but die after failing to involute their heads.

Unlike the shortened trachea of the previously characterized *uif* and *Mmp1*, we recovered four mutant lines with large, convoluted trachea in both their dorsal trunks and secondary branches (*I(3)LL9349*, *I(3)LL16674*, *I(3)LL10756*, and *I(3)LL12265*). Complementation tests show that *I(3)LL9349*, *I(3)LL16674* and *I(3)LL10756* map to the same complementation group while *I(3)LL12265* is found in its own complementation group. We observed that all four of these mutants have an extended larval life (Figure 5). Although the mutants initially show a greater degree of embryonic lethality, they continue to persist as larvae well past the normal time of pupariation of their control heterozygous sibling. Due to hypoxic behavior of mutant larvae wandering away from food, we checked the animals for secondary symptoms of hypoxia. Upon dissection, the overgrowth mutants all lack imaginal discs and have small brains (Figure 6).

The overgrowth mutants all initially have similar body sizes to their heterozygous siblings throughout the first, second and early third instar. However, at the time of their lethality, their

body sizes are smaller than those of late third instar controls and their trachea have largely overgrown to fill their bodies (Figure 4).

We measured the partial trachea to body length ratio in these mutants to better understand the growth trajectory of the trachea. The mutants follow the growth of their heterozygous sibling controls closely throughout the first three days of larval growth. Upon normal pupariation by the controls, the mutants drastically increase their partial trachea to body length ratio in the following day (Figure 7). Rather than a continuous faster rate of growth throughout the larval life, these mutants show a punctuated growth at the beginning of their extended larval life.

Cloning of rio

We selected the multiallelic complementation group composed of *I(3)LL9349*, *I(3)LL10756* and *I(3)LL16674* for gene mapping because it was the only group with more than one allele and it produced a phenotype opposite to the previously characterized positive regulators of growth *uif* and *Mmp1*. Based upon having 3 EMS-induced alleles we believe it is likely that this gene is a negative regulator of larval tracheal growth. We named this gene *rio* due to the convolutions the trachea makes through the larval body reminding us of a river.

We performed whole genome sequencing on all seven mutant alleles. There was no obvious gene candidate with high (stop gained, frameshift, start lost, splice site acceptor/donor) effect hits present in all *rio* alleles. Therefore, we sorted the sequencing data from the three alleles into high and moderate effects (non-synonymous coding, splice site region, codon deletion/insertion), and filtered the sequence files for homozygous variants in the DGRP collection through FlyVar (Wang et al., 2015). We then conducted complementation tests with deficiencies that mapped to any region that contained a gene with more than one allele with high or moderate effect mutations. Screening of 18 different deficiency stocks throughout the

third chromosome revealed three regions that failed to complement with at least one *rio* allele. Only one deficiency stock, *Df(3R)BSC793*, failed to complement all three *rio* alleles.

Df(3R)BSC793 was rebalanced over *TM6, Dfd>YFP* so mutant larva could be selected and analyzed for trachea overgrowth phenotypes.

Complementation of *Df(3R)BSC793* with the *rio* alleles recapitulated the convoluted tracheal phenotype (Figure 8). This deficiency encompasses the far right arm of the third chromosome from 3R:31,200,119 to 3R:31,458,140, spanning 28 different genes on the far right arm of the 3rd chromosome. A second deficiency, *DF(3R)BSC749* was able to narrow this region down to the right half of *DF(3R)BSC793*. We performed tracheal specific RNAi knockdown with *btl* for all available RNAi lines in this region, and the majority of RNAi lines showed no significant phenotypic change. One line (*TRiP.HMS02694*) showed trachea of normal size but frequent breaks. Only knockdown by *CG11340 (btl-GAL4 x TRiP.JF02028)* caused a similar phenotype to the *rio* mutants with large, convoluted trachea. Transheterozygotes of *rio* alleles with the *Mi{MIC}CG11340^{M11939}* allele produced similar phenotypes, confirming the identity of the *rio* gene as *CG11340* (Figure 8). The sequencing data for the *rio* alleles show mutations in an intron and upstream of the *CG11340* gene in the mutants. The *Mi{MIC}* insertaion is also found in the *CG11340* intron.

Rio is encoded by *CG11340*

The predicted *rio* gene, *CG11340*, encodes a 526 amino acid protein with a molecular mass of ~60 kDa. The protein contains an extracellular region from amino acids 1 to 298 followed by three transmembrane passes, a small intracellular region from amino acids 385 to 505 and an additional transmembrane pass (based on TMHMM, Krogh et al., 2001) (Figure 9). The *CG11340* protein is predicted to be a ligand-gated chloride channel used in neurotransmission (Witte et al., 2002). Interestingly, genome-wide spatial and temporal

expression information (<http://flybase.org>) and ModEncode (CONSORTIUM et al. 2010) indicate that *CG11340* is not only expressed in the brain but also in moderate levels in non-neuronal tissues such as the midgut and malpighian tubules, and its mRNA is present from late embryogenesis until pupariation, raising the possibility that Rio may be expressed in non-neural tissues and have an effect during the larval life.

A BLASTP search revealed that the closest human ortholog to Rio is GLRA2, a subunit of the glycine receptor chloride channel. Sequence alignment in HHpred also showed functional prediction to the GLRA2 protein with 100% probability between the GLRA2 aa35-444. Most notably, the transmembrane domains are conserved between the two proteins. The site at GLRA2 aa295 that is important in the closed conformation in ion obstruction is conserved between the two proteins (UniProt 2009) (Figure 10).

Rio acts tissue-autonomously in the trachea for growth

We wanted to determine whether the *rio* gene acted in a tracheal tissue specific manner (similar to *uif*) or if it would have an effect on all body tissues. We performed a series of tissue-specific RNAi experiments in various tissues with *rio*-RNAi to address this question. We used the *engrailed* driver to knockdown *rio* (*en-Gal4>UAS-CG11340 RNAi*) specifically in the posterior compartment of the wing imaginal discs (Figure 11) and *apterous* (*ap-Gal4>UAS-CG11340 RNAi*) to knockdown in the dorsal compartment (data not shown). Our dissection of late third instar imaginal discs showed no significant difference in cell size between the affected and control compartments in the posterior compartment of the wing discs. The adults eclosed normally and displayed normal adult wings.

We observed the tracheal phenotype in a knockdown of *CG11340* in the trachea (*btl-Gal4>UAS-CG11340 RNAi*) in the late larval life. Ubiquitous knockdown of *CG11340* (*da-Gal4>UAS-CG11340 RNAi*) produced larvae with a smaller degree of tracheal overgrowth in the

dorsal trunks but pronounced overgrowth in the secondary branches (Figure 8). The bodies of these larvae are of normal size and the majority of the animals pupariate and become viable adults. In our experiments looking at *rio*'s effect in tissue specific growth, we believe that *rio* is specific to the growth of the trachea.

Characterization of rio phenotypes

We wanted to better understand why the body size of the larva is smaller than their heterozygous siblings. Following a normal first and second instar of body size compared to controls, the *rio* mutants begin to slow in body length growth during the third instar. Even though these larvae continue to live past the time of normal pupariation, their terminal body size is still smaller than a control late 3rd instar larva. Upon dissection during the late third instar, we observed that the *rio* mutants were lacking imaginal discs and have significantly smaller brains (Figure 6). The *rio* mutants also wander away from their food and crawl to the outer edges of the agar plates and have smaller accumulations of fat. Hypoxia is consistent with these observed phenotypes (Wingrove and O'Farrell, 1999).

Since *rio* impacts larval trachea growth in a similar (but opposite) manner compared to *uif* and *Mmp1*, we were interested to know if they had an effect on each other within the cell. We stained the *rio* mutants' trachea with both Uif and Mmp1 antibodies to characterize *rio*'s impact on the pathway that includes Uif and Mmp1. Interestingly, the *rio* mutants showed an overall Uif protein upregulation at the cell membranes in the tracheal tissue. We observed a mosaic pattern of multiple cells in each metamere that was highly upregulated with Uif throughout the cell. Our staining with Mmp1 showed the same mosaic pattern (Figure 12).

During the study of *uif*, *Mmp1*, and *rio*, we noticed an interesting nuclear phenotype in the mutant trachea. Control trachea contain squamous cells with nuclei spread evenly

throughout the trachea. In the mutants, although the cell outlines appear normal after staining with Coracle and DAPI, the nuclei are all grouped on the edge of the trachea. This phenotype appears to be an artifact of the fixation process. When the trachea are stained with only DAPI in a PBS+Tween+NDS buffer, the nuclei are spread evenly throughout the trachea (Figure 13).

Neither cellular or aECM organization appears to be disrupted in the *rio* mutants. Cells of the *rio* mutants maintain their normal polygonal shape while maintaining clear cellular borders to their neighbors. The taenidia of the *rio* mutants also maintain their integrity. In both the *uif* and *Mmp1* mutants, taenidia have been shown to have a disrupted, wavy phenotype. The number and spacing of taenidia in the *rio* mutants also does not appear to change (Figure 14). Cell number in each metamere and cellular size remains consistent between *w¹¹¹⁸* and *rio* mutants (data not shown).

DISCUSSION

Here we have described the initial identification and characterization of seven EMS-derived mutants that show growth phenotypes in the larval trachea. The organization and size of the trachea in all of these mutants appear normal immediately following embryogenesis, but either follow a trajectory of overgrowth or undergrowth during their larval life. Previously, *uif* and *Mmp1* have been characterized in the literature to be positive regulators of growth, causing significantly smaller trachea in the mutant larvae (Zhang et al., 2009; Glasheen et al., 2010). In this work we found four mutants that also likely act as positive regulators of growth with all of them mapping to unique loci on the third chromosome. Interestingly, we also found four mutations that result in a tracheal overgrowth phenotype, suggesting that they may encode negative regulators of tracheal growth. We chose to characterize one of these genes that had three alleles (*I(3)LL9349*, *I(3)LL16674* and *I(3)LL10756*). We named this gene *rio* based upon its convoluted tracheal phenotype. As a negative regulator of growth, *rio* may help us to understand how positive regulators such as *uif* and *Mmp1* provide tissue specific growth regulations in the larval trachea.

Multiple pieces of evidence point to *CG11340* as being the gene encoding Rio. We observed that the *Df(3R)BSC793* deficiency failed to complement any of the *rio* alleles. With any EMS mutagenesis, it is likely to have multiple lethal mutations on a chromosome. Failure to complement an allele is not necessarily an indication that the region contains the mutation of interest, however, since all three mutants failed to complement in this region, we are quite certain that the *rio* gene is present here. Additionally, knockdown with *CG11340* RNAi in the trachea recapitulated the tracheal overgrowth phenotype where knockdown with the other RNAi lines found in this region did not give a tracheal phenotype. Finally, transheterozygotes with the

insertion *Mi{MIC}CG11340^{MI11939}* allele which was inserted into the *CG11340* exon also show tracheal overgrowth.

We show a unique tissue specific growth function in the trachea for the *rio* gene in these studies. Tissue specific knockdown by RNAi of *rio* in the trachea causes the same overgrowth phenotype seen in the *rio* mutants whereas knockdown in other tissues causes no overgrowth phenotype. Interestingly, ubiquitous knockdown of *rio* produces larvae with normal sized bodies but the trachea in these larvae have a larger diameter in the dorsal trunks and convoluted secondary braches. These results lead us to conclude that the *rio* gene is essential as a tissue-specific negative growth regulator in the trachea since it does not appear to have an effect on growth control in the other tested tissues.

In the RNAi knockdown experiments, the tracheal overgrowth phenotype produce was less pronounced than in the EMS-produced *rio* mutants. The RNAi may not have produced a complete knockdown or combined with off-target effects. Alternatively, the loss-of-function *rio* alleles could perform regulatory mechanisms that are not affected in RNAi knockdown. A weaker phenotype in the trachea could result in a lessened effect to its gas-exchanging function. If the trachea in these animals are able to transport gases to the body tissues, the secondary effects of hypoxia including defects to organism size would be lessened (Wingrove and O'Farrell, 1999). This could explain the larger bodies of the ubiquitously expressed *CG11340*.

Functions of rio in the larvae

The *rio* gene has previously been shown to encode a ligand-gated chloride channel subunit in *Drosophila* (Witte et al., 2002). Besides functioning as a neurotransmitter, two other functions have been described in the literature. Remnant et al. (2014) showed that the Rio protein is highly expressed in non-neural tissues including the malphigian tubules and midgut. Based on GFP expression studies, Rio appears to have the highest expression in the copper

cell region of the midgut. Here it was found that the loss of *rio* caused an increased tolerance to copper in the mutants. It was predicted that loss of *rio* in the gut could reduce the acidity in the gut leading to a reduced copper uptake and a higher tolerance to dietary copper. A second place of non-neuronal tissue expression was found in the *Drosophila* renal tubule. High expression of *rio* mRNA was found along with a second ligand-gated chloride channel-like protein (CG7589) leading them to conclude it was functioning as a chloride channel in this tissue (Wang et al., 2004).

The human ortholog of *rio* is the GLRA2 gene that encodes the alpha-2 subunit of the glycine receptor chloride channel (GlyR Cl⁻). The GlyR Cl⁻ channel is abundantly expressed in the spinal cord where it functions to hyperpolarize the membrane by conducting chloride ions. Non-neuronal expression of these channels has also been found in human macrophages, endothelial cell and certain endocrine glands. Interestingly, GlyR Cl⁻ expression was found on airway smooth muscle cells where they are predicted to facilitate relaxation of the airway smooth muscle (Yim et al. 2011). Since the larval trachea is analogous to the mammalian lung, it follows that Rio may be functioning in the described non-neurotransmitter role in the larval trachea. Relaxation of tracheal tissue by the Rio channel could potentially allow for the loss of rigidity needed as a signal to halt growth. Without this tissue feedback, growth could continue leading to the overgrowth phenotype in the mutants.

Interaction of rio with known tracheal growth effectors

The *rio* mutants displayed interesting staining patterns for antibodies against Uif and Mmp1 in the cells of the overgrown trachea. We observed that Uif staining was generally overexpressed throughout the *rio* tissues compared to *w¹¹¹⁸*. We also have shown the existence of a clear mosaic pattern in which arbitrary cells throughout the trachea are highly upregulated for Uif and Mmp1. These cells express notably higher concentrations of Uif and Mmp1 than

other surrounding cells next to them. Since *Mmp1* and *Uif* are both required at the cellular membrane for related function during the degradation and remodeling of the aECM during molts, it is possible that the dual overexpression of these genes is linked. Furthermore, since the regulatory network governing tracheal growth has been perturbed by the loss-of-function *rio* gene product, it is possible that the mutant growth pathway exhibits extreme variation in gene expression.

Unlike the aECM of the *uif* and *Mmp1* mutants, the *rio* mutants showed no sign of taenideal disorganization. Since both positive regulators of growth are involved in stabilizing the aECM and cuticle degradation, it follows that organization of the taenidia would be disrupted without them. It is clear that both *Uif* and *Mmp1* are present in *rio* mutants, in overexpressed quantities shown by antibody staining, allowing for proper aECM organization. It may be that it is the extra tracheal tissue in the overgrowth mutants that is causing overexpression of *Uif* and *Mmp1*. As the trachea of the *rio* mutants grows past the intrinsically set tissue length of a normal larva, more aECM organization is likely needed. Proteins that function in the organization of aECM, like *Uif* and *Mmp1*, may be upregulated to manage the new increased amount of growth.

How might *rio* interact with *uif* and *Mmp1* to genetically control growth in the trachea? One hypothesis is that *rio* is involved in the trafficking and recycling of membrane proteins including *Uif* and *Mmp1*. The loss-of-function alleles of *rio* correlate with higher amounts of *Uif* and *Mmp1* at the cellular membrane. Accumulations of these positive growth regulating proteins at the membrane may be the cause of the increase in tracheal size of the *rio* mutants.

We plan to create an antibody specific to the *Rio* protein since it will be crucial to identify where and when *Rio* is located in the tracheal cells. Understanding its physical and genetic interactions with the positive growth effectors *Uif* and *Mmp1* will elucidate more general phenomena in metazoan tissue specific growth regulation.

REFERENCES

1. Beitel, G.J. and M.A. Krasnow, *Genetic control of epithelial tube size in the Drosophila tracheal system*. Development, 2000. 127(15): p. 3271-3282.
2. Britton, J.S., 2000 Genetic and environmental control of growth and the cell cycle during larval development of *Drosophila melanogaster*. Ph.D. Thesis, University of Washington.
3. Consortium, T. m., S. Roy, J. Ernst, P. V. Kharchenko, P. Kheradpour et al. *Identification of functional elements and regulatory circuits by Drosophila modENCODE*. Science, 2010. 330, 1787-1797.
4. Egeblad, M., Werb, Z., *New functions for the matrix metalloproteinases in cancer progression*. Nat. Rev. Cancer, 2002. 2, 161–174.
5. Glasheen, B.M., R.M. Robbins, C. Piette, G.J. Beitel, and A. Page-McCaw, *A matrix metalloproteinase mediates airway remodeling in Drosophila*. Dev. Biol., 2010. 344(2): p. 772-783.
6. Hall, S., Bone, C., Oshima, K., Zhang, L., McGraw, M., Lucas, B., Fehon, R. G., Ward, R. E. *Macroglobulin complement-related encodes a protein required for septate junction organization and paracellular barrier function in Drosophila*. Development, 2014. 141, 889-898.
7. Krogh, A., Larsson, B., von Heijne, G., Sonnhammer, E.L., *Predicting transmembrane protein topology with a hidden Markov model: application to complete genomes*. J. Mol. Biol., 2001. 305, 567–580.

8. Liu, L., Johnson, W.A., Welsh, M.J. *Drosophila* DEG/ENaC pickpocket genes are expressed in the tracheal system, where they may be involved in liquid clearance. Nat. Academy of Sciences, 2002. 100, 2128-2133.
9. Makino, S., *A morphological study of the nucleus in various kinds of somatic cells of Drosophila virilis*. Cytologia, 1938. 9: p. 272-282.
10. Manning G, Krasnow MA. 1993. Development of the *Drosophila* tracheal system. In: Bate M, Martínez-Arias A, editors. The development of *Drosophila melanogaster*. Cold Spring Harbor, NY: Cold Spring Harbor Laboratory Press. pp 609-685.
11. Matussek, T., Djiane, A., Jankovics, F., Brunner, D., Mlodzik, M., Mihaly, J. *The Drosophila formin DAAM regulates the tracheal cuticle pattern through organizing the actin cytoskeleton*. Development, 2006. 133, 957–966.
12. Metzger, R. J. and Krasnow, M. A. *Genetic control of branching morphogenesis*. Science, 1999. 284, 1635-1639.
13. Page-McCaw A, Serano J, Sante JM, Rubin GM. *Drosophila* matrix metalloproteinases are required for tissue remodeling but not embryonic development. Dev Cell. 2003, 4(1):95-106.
14. Pelabon, C. *et al*. Evolution of morphological allometry. *Ann. N.Y. Acad. Sci.* 2014. 1320, 58–75.
15. Rasband, W.S., 1997-2009. ImageJ. National Institutes of Health, Bethesda, MD, USA.

16. Remnant, E.J., Williams, A., Lumb, C., Yang, Y.T., Chan, J., Duchenet, S., Daborn, P.J., Battersham, P., Perry, T. *Evolution, expression, and function of non-neuronal ligand-gated chloride channels in Drosophila melanogaster*. *G3*, 2014. 1-16.
17. Sternlicht, M.D., Werb, Z., *How matrix metalloproteinases regulate cell behavior*. *Annu. Rev. Cell Dev. Biol.*, 2001. 17, 463–516.
18. Uhlen M, Oksvold P, Fagerberg L, Lundberg E, Jonasson K, Forsberg M, Zwahlen M, Kampf C, Wester K, Hober S, Wernerus H, Björling L, Ponten F. *Towards a knowledge-based Human Protein Atlas*. *Nat Biotechnol*. 2010 28(12):1248-50.
19. UniProt Consortium 2009, GLRA2_Human, *UniProtKB Protein Knowledgebase*, viewed 28 June 2016 <<http://www.uniprot.org/uniprot/P23416>>.
20. Wang, F., Jiang, L., Chen, Y., Haelterman, N.A., Bellen, H.J., Checn, R. *FlyVar: a database for genetic variation in Drosophila melanogaster*. *Database*, 2015. p. bav079.
21. Wang, J., Kean, L., Yang, J., Allan, A.K., Davies, S.A., Herzyk, P., Dow, J.A.T. *Function-informed transcriptome analysis of Drosophila renal tubule*. *Genome Biology*, 2004. 5, 1-21.
22. Wang, L., Evans, J., Andrews, H. K., Beckstead, R. B., Thummel, C. S. and Bashirullah, A. *A genetic screen identifies new regulators of steroid- triggered programmed cell death in Drosophila*. *Genetics*, 2008. 180, 269-281.
23. Wingrove, J. A., and O'Farrell, P. H. *Nitric oxide contributes to*

behavioral, cellular, and developmental responses to low oxygen in Drosophila.

Cell 1998. 12, 105–114.

24. Wingrove, J.A., O'Farrell, P.H., *Nitric oxide contributes to behavioral, cellular, and developmental responses to low oxygen in Drosophila.* Cell, 1999. 98, 105–114.

Wu,

25. Witte, I., Kreienkamp, H.J., Gewecke, M., Roeder, T. *Putative histamine-gated chloride channel subunits of the insect visual system and thoracic ganglion.* J. Neurochem. 2002. 83(3), 504-514.

26. Xie, G., Zhang, H., Du, G., Huang, Q., Liang, X., Ma, J., and Jiao, R. *Uif, a large transmembrane protein with EGF-like repeats, can antagonize Notch signaling in Drosophila.* PLoS ONE, 2012. 7, e36362.

27. Yim, P.D., Gallos, G., Xu, D., Zhang, Y., Emala, C.W. *Novel expression of a functional glycine receptor chloride channel that attenuates contraction in airway smooth muscle.* FASEB J. 2011. 25:1706-1717.

28. Zhang L, Ward R. 2009. *uninflatable encodes a novel ectodermal apical surface protein required for tracheal inflation in Drosophila.* Dev. Biol., 2009. 336, 201-212.

TABLES AND FIGURES

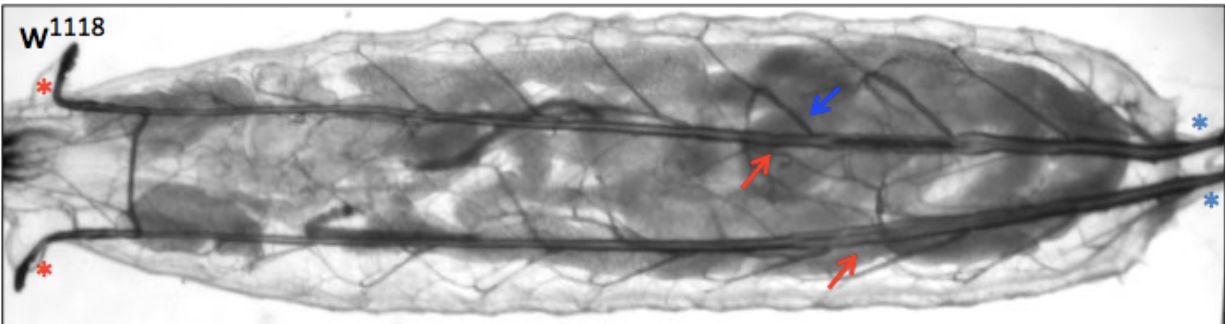


Figure 1. The trachea branches throughout the body to act as the respiratory organ
The trachea opens to the outside of the animal at both the anterior (red asterisks) and posterior (blue asterisks) spiracles. Two large dorsal trunks (red arrows) run through the animal. Secondary branches (blue arrow) divide from the dorsal trunk and repeatedly branch into finer branches that reach the body tissues.

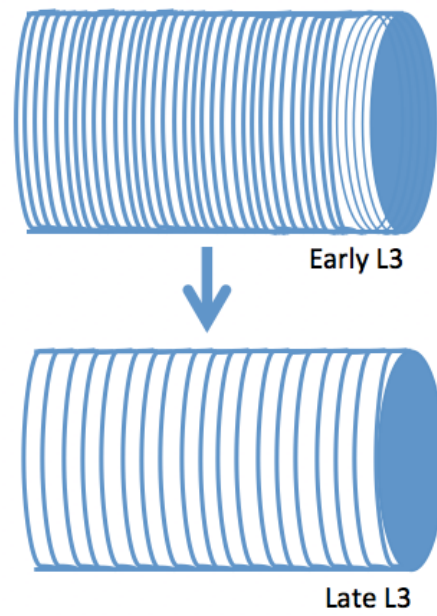


Figure 2. Taenideal spacing expands during instars

Taenideal ridges are close together at the beginning of an instar. As the larva grows, space is added between the ridges.

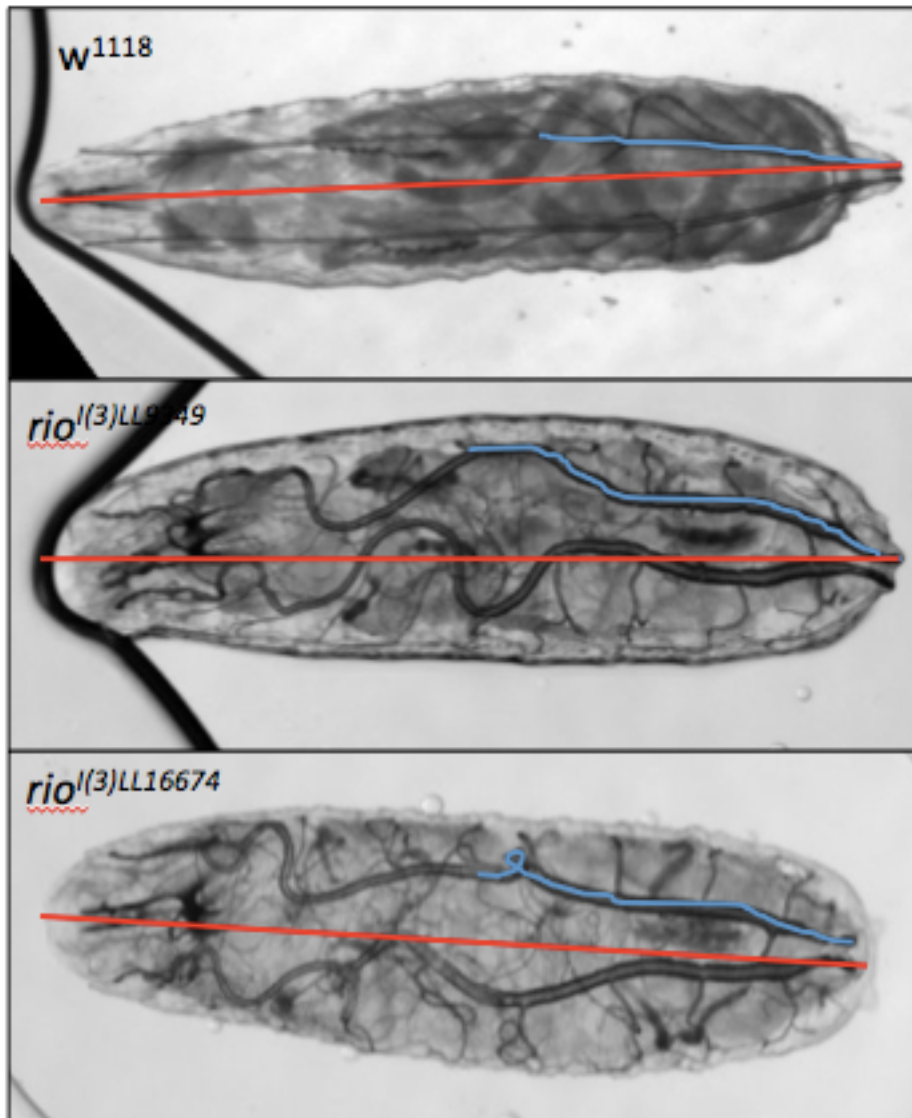


Figure 3. Partial trachea length to body length ratios are used to quantify the amount of tracheal overgrowth in *rio* mutants

We determined the partial trachea length by measuring the distance from the posterior spiracles to the transverse connective that was established in body segment four (blue lines). The total body length was measured as the most anterior point to the most posterior point of the animal (red line).

Allele(s)	Tracheal Phenotype	Terminal size	Penetrance
<i>I(3)LL15149</i>	Short trachea, frequent breaks	small	High
<i>I(3)LL16636</i>	Short trachea	small	Low
<i>I(3)LL5106</i>	Short trachea	medium	Mid
<i>I(3)LL12265</i>	Convolutated trachea	medium	Mid
<i>I(3)LL9349,</i> <i>I(3)LL10756,</i> <i>I(3)LL16674</i>	Highly convolutated trachea	medium	High

Table 1. Collection of larval lethal mutants with tracheal-specific growth defects

From a collection of 252 larval lethal mutants, 7 were found to have phenotypes specific to their tracheal growth. The 7 EMS stocks identified comprise 5 unique complementation groups. Three of these stocks (*I(3)LL15149*, *I(3)LL16636*, and *I(3)LL5106*) produce small, shortened trachea similar to the *uif* and *Mmp1* phenotypes. Stock *I(3)LL15149* is unique in that it produces breaks in the trachea. All of the small trachea mutants (*I(3)LL15149*, *I(3)LL16636*, and *I(3)LL5106*) show a terminal size smaller than the *w¹¹¹⁸* sizes. The other four stocks (*I(3)LL12265*, *I(3)LL9349*, *I(3)LL10756* and *I(3)LL16674*), comprising two complementation groups, have large convoluted trachea with a high penetrance. The stocks have varying levels of penetrance.

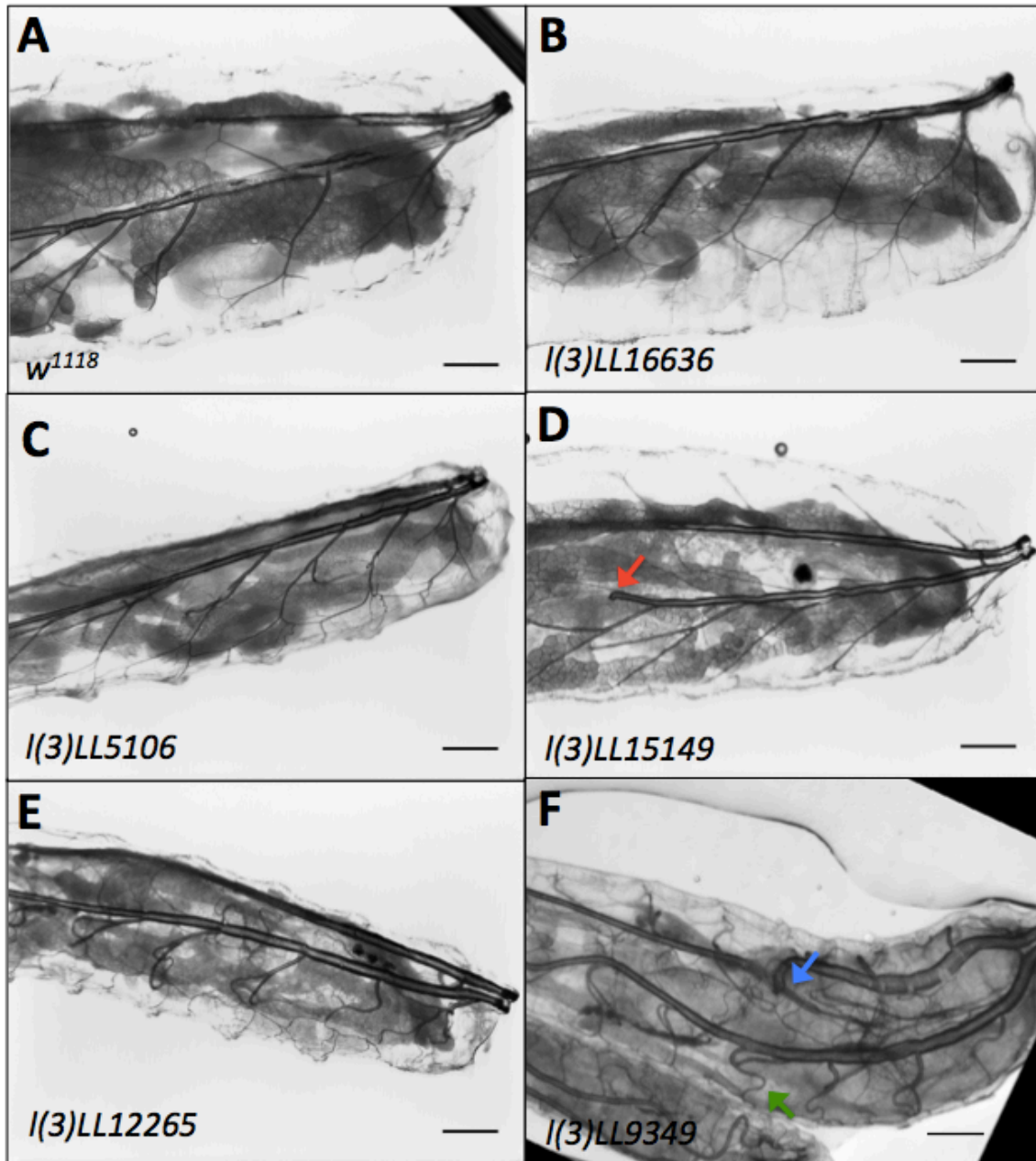


Figure 4. Collection of EMS-induced mutants show tracheal specific growth phenotypes
 Brightfield photomicrographs of mutant lines collected from the low-dose EMS mutagenesis screen for larval trachea effectors (five shown here). Both positive and negative tracheal growth effectors were isolated. Mutants *I(3)LL16636* (B), *I(3)LL5106* (C) and *I(3)LL15149* (D) (along with *I(3)LL16674* and *I(3)LL10756* not shown) showed smaller trachea compared to *w¹¹¹⁸* (A). Interestingly, *I(3)LL15149* (D) showed frequent breaks within the growing trachea (red arrow). Mutants *I(3)LL12265* (E) and *I(3)LL9349* (F) (along with *I(3)LL10756* and *I(3)LL10756* not shown) have larger, convoluted trachea compared to *w¹¹¹⁸* (A). Line *I(3)LL9349* have trachea that often become so convoluted that they fold over on themselves (blue arrow). They also have convolutions in their secondary branches (green arrow). Scale bar = 200 μ m.

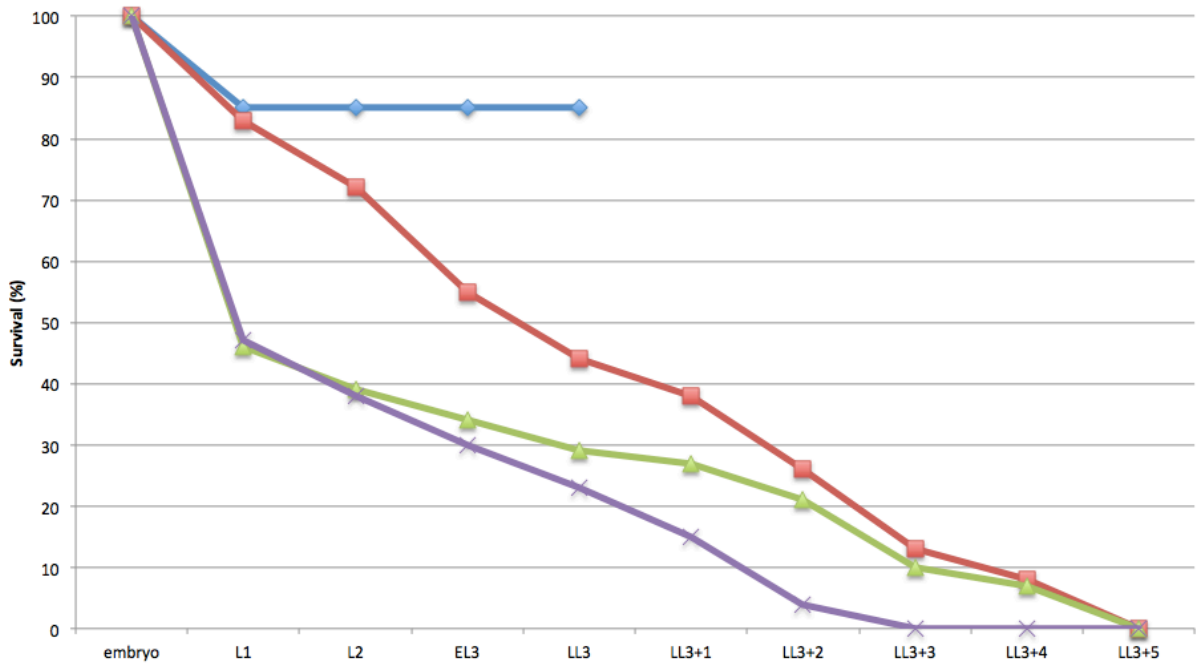


Figure 5. Overgrowth mutants have extended larval lives

rio mutants are larval lethal but have an extended larval life. *w¹¹¹⁸* (blue) animals hatch after one day of embryogenesis, followed by four days of larval growth before pupariating into prepupa at LL3. The *rio¹⁶⁶⁷⁴* (green) and *I(3)LL12265* (purple) mutants show an increase in embryonic lethality (~55%) while the *rio⁹³⁴⁹* mutants have a nearly identical amount of embryonic lethality as the *w¹¹¹⁸*. The *rio* mutants persist as larva past the normal time of pupariation at day 4 but are all dead by 5 days after pupariation (LL3+5) should have taken place. (*w¹¹¹⁸*, n=100; *rio⁹³⁴*, n=156; *rio¹⁶⁶⁷⁴*, n=184, *I(3)LL12265*, n=100)

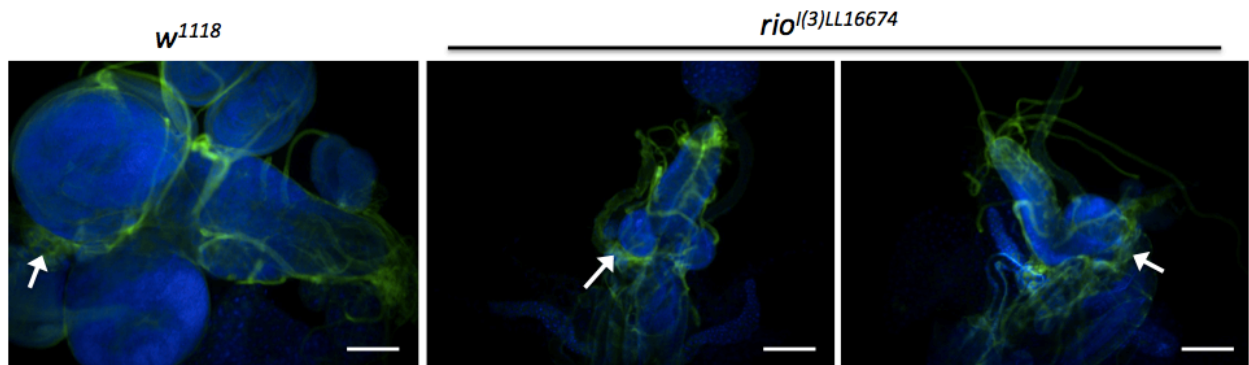


Figure 6. *rio* mutants have small brains at the time of lethality

The brains of the *rio* mutants near lethality (B,C) are significantly smaller upon dissection than the brains of *w¹¹¹⁸* at LL3 (A). Brains stained with DAPI (blue) and anti-Cor (green). White arrows indicate anterior lobes. Scale bars = 110 μ m

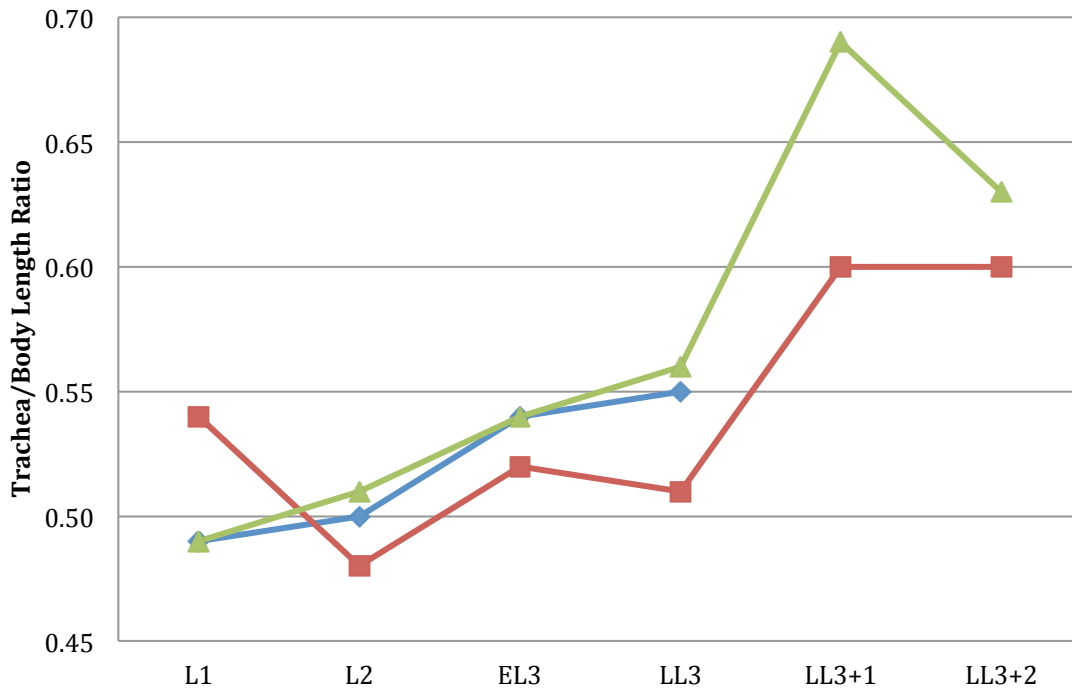


Figure 7. Partial trachea to body length ratios are higher in *rio* mutants during the extended larval life

Partial trachea length was calculated as the distance along the dorsal trunk from the posterior spiracle to the transverse connective that originated in body segment 4. The trachea to body length ratios stay consistent between *w*¹¹¹⁸ (blue), *rio*⁹³⁴⁹ (red), and *rio*¹⁶⁶⁷⁴ (green) during the first four days of larval growth (L1-LL3). Upon pupariation of *w*¹¹¹⁸, the ratio of the *rio* mutants increases dramatically. No significant difference in tracheal growth rate was found between the *w*¹¹¹⁸ and *rio* mutant phenotypes based on linear regression analysis.

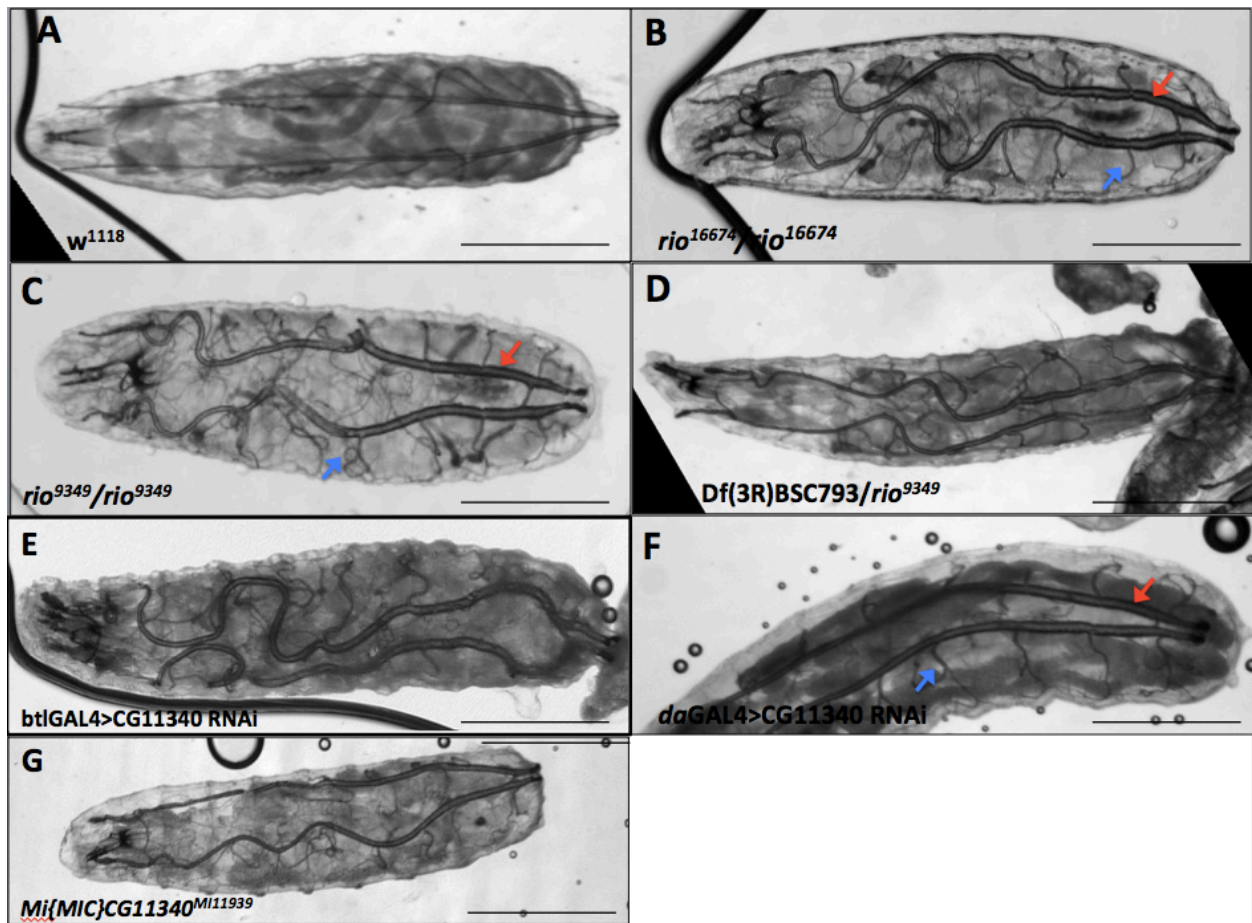


Figure 8. *rio* mutant larvae have overgrown tracheas during the extended third instar Brightfield microphotographs show both tracheal overgrowth mutants *rio*¹⁶⁶⁷⁴ (B) and *rio*⁹³⁴⁹ (C) with highly convoluted trachea compared to *w*¹¹¹⁸ (A). Convulsions are found in both the dorsal trunks (red arrows) of the trachea and the secondary branches (blue arrows). The trachea become so convoluted in some regions that they fold over on themselves. This overgrowth phenotype was recapitulated when *rio*⁹³⁴⁹ was crossed to the Bloomington deficiency stock *Df(3R)BSC793* (D). Tracheal specific knockdown of *CG11340* using the *btl* driver gave a convoluted phenotype like the *rio* mutants (E). Ubiquitous knockdown of *CG11340* shows slight enlargement in the dorsal trunks and convulsions in the secondary branches (F). The Mi{MIC} insertion allele shows similar convoluted trachea (G). Scale bars = 1000 μ m.

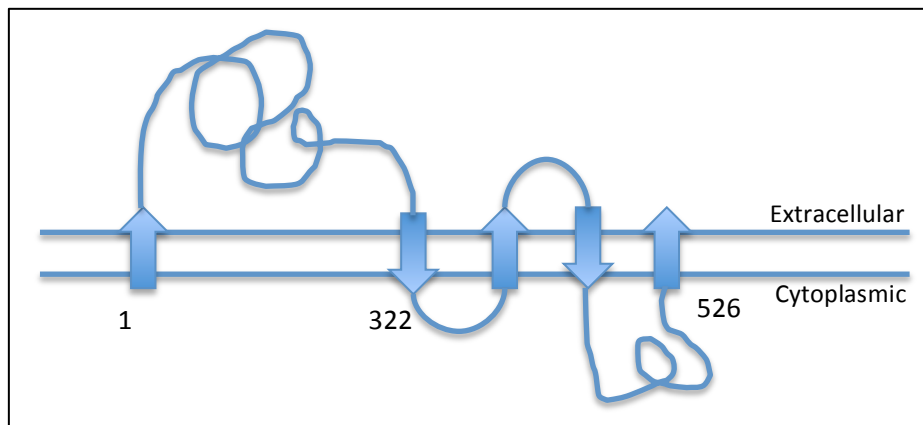


Figure 9. Predicted transmembrane domains of the Rio protein

Based on transmembrane helix prediction (TMHMM), the *rio* gene encodes a protein with an extracellular region from amino acids 1 to 298 followed by three transmembrane passes, a small intracellular region from amino acids 385 to 505 and an additional transmembrane pass.

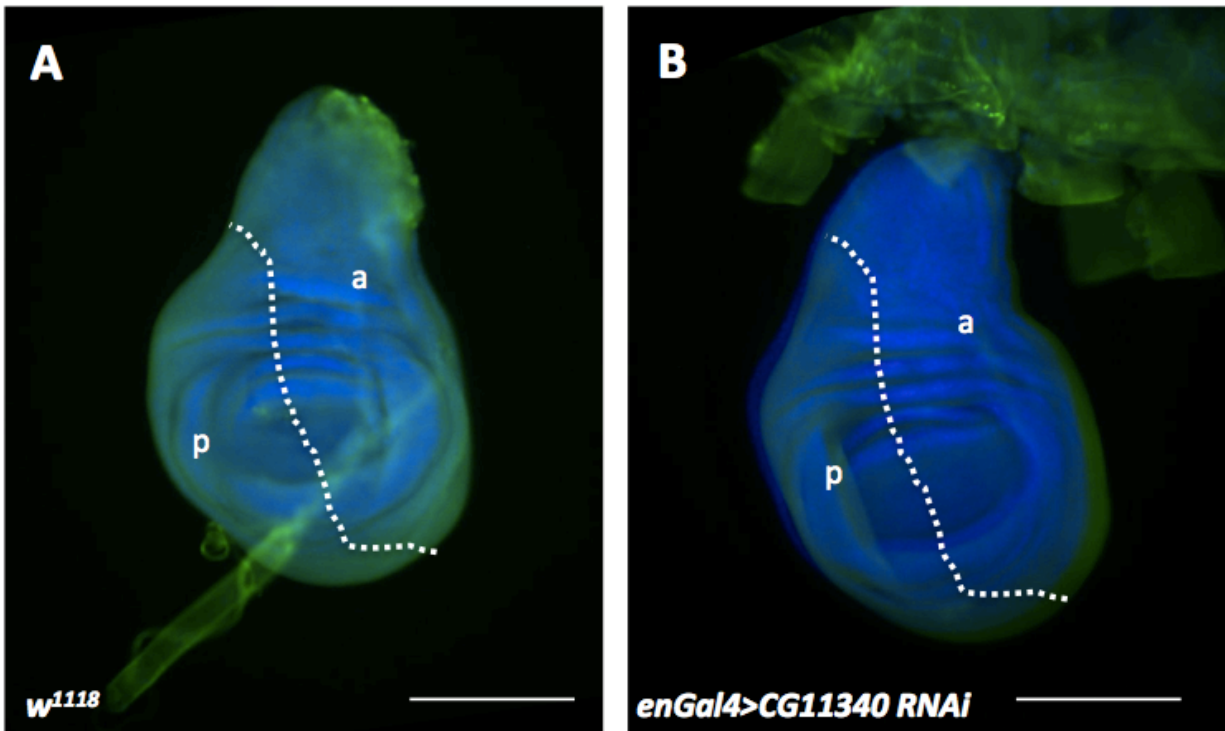


Figure 11. Knockdown of *rio* in the wing imaginal disc shows no effect on tissue growth
Tissue specific RNAi knockdown of *CG11340* in the posterior compartment (p) of the wing imaginal disc (B) shows no difference in cellular growth to wildtype posterior segment (A) stained with anti-Cor (green) and DAPI (blue). White line indicates the anterior/posterior boundary. Scale bars = 220 μ m, n=5.

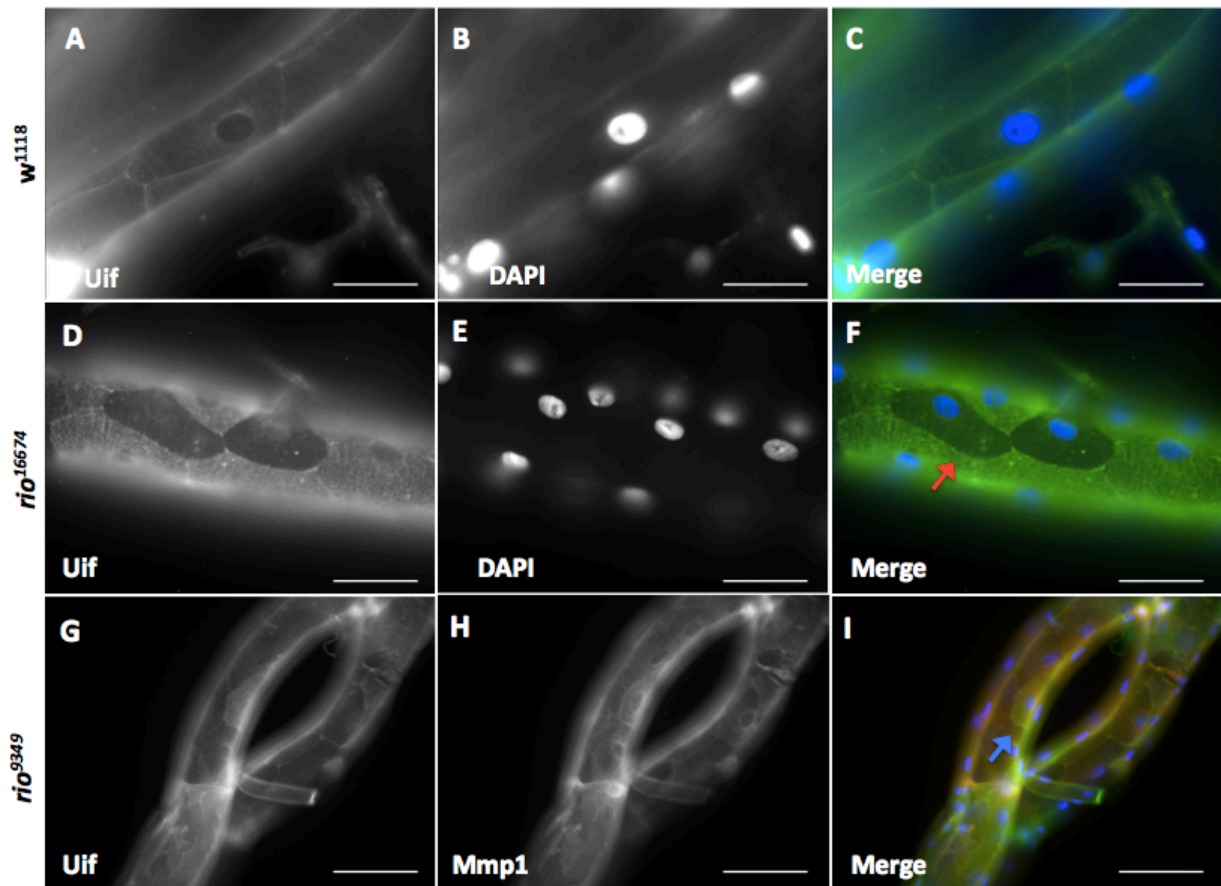


Figure 12. *rio* mutants show a cellular mosaic pattern of both Uif and Mmp1 upregulation
 Confocal micrographs of *rio* trachea show a clear cellular mosaic pattern with some cells highly expressing anti-Uif (D and F, green) next to cells of normal expression (red arrow) compared to anti-Uif staining in *w¹¹¹⁸* (A and C, green). Cells shown The mosaic cells that are highly expressing Uif (G and I, green) are also highly expressing Mmp1 (H and I, red, blue arrow). Scale bar = 50 μ m.

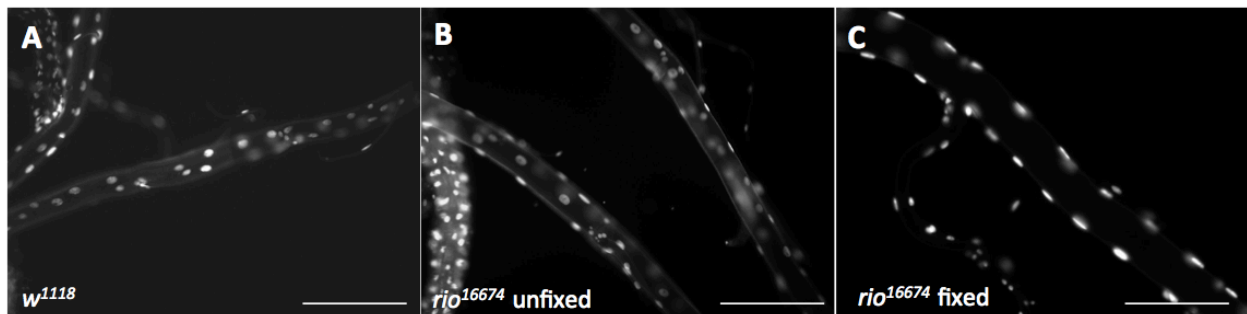


Figure 13. Nuclear crowding phenotype in tracheal mutants is a result of fixation

Nuclei stained with DAPI in the *rio¹⁶⁶⁷⁴* mutant following standard fixation with 4% paraformaldehyde crowd along the sides of the trachea (C) compared to the *w¹¹¹⁸* trachea with the nuclei spread evenly throughout the trachea (A). The *rio* mutant produces the normal evenly distributed nuclei in the trachea when it is stained with DAPI without fixation (B). Scale bars = 220 μ m.

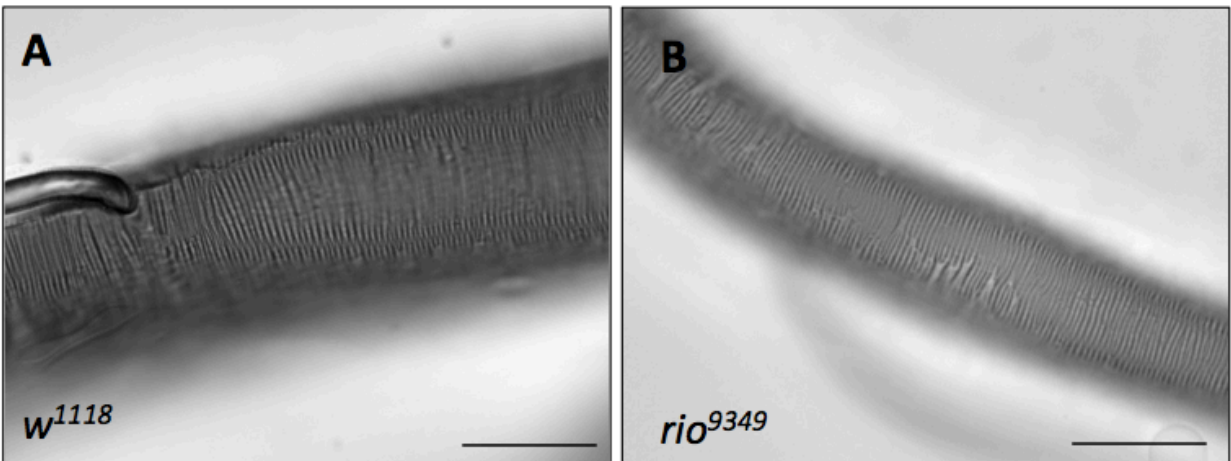


Figure 14. aECM organization is not disrupted in *rio* mutants

Brightfield micrographs of organized taenidial ridges can be seen running perpendicular along the axis of the trachea in both the *w¹¹¹⁸* (A) and *rio⁹³⁴⁹* (B) trachea. Scale bars = 50 μ m.